www.czasopisma.pan.pl PAN POLSKA AKADEMIA NAUK www.journals.pan.pl

Arch. Metall. Mater. **67** (2022), 4, 1305-1314

DOI: https://doi.org/10.24425/amm.2022.141056

B. KRASOWSKI[1], A. KUBIT[2], T. TRZEPIECIŃSKI[2*], J. SLOTA[3]

MANUFACTURE OF BEAD-STIFFENED PANELS USING THE SINGLE POINT INCREMENTAL SHEET FORMING TECHNIQUE

This paper presents the results of experimental research on the fabrication of thin-walled panels with longitudinal stiffening ribs by the single point incremental sheet forming technique. The bead-stiffened panels were made of Alclad 2024-T3 aluminium alloy sheets commonly used in aircraft structures. The influence of forming parameters and tool strategy on surface quality and the possibility of obtaining stiffening ribs with the required profile and depth was tested through experimental research. Two tool path strategies, spiral with continuous sinking and multi-step z-level contouring, were considered. The results of the experiments were used to verify the finite element-based numerical simulations of the incremental forming process. It was found that the main parameter which influences the formability of test sheets is the tool path strategy; the tool path strategy with multi-step z-level contouring allowed the rib to be formed to a depth of 3.53 mm without risk of cracking. However a greater depth of rib equal of 5.56 mm was achieved with the continuous tool path. The tool path strategy was also the main parameter influencing the surface finish of the drawpiece during the single point incremental forming process.

Keywords: aluminium alloy; incremental sheet forming; numerical modelling; thin-walled structure

1. Introduction

Incremental sheet forming (ISF), also known as Single Point Incremental Forming (SPIF), is a manufacturing technique where a piece of thin sheet metal blank is shaped into a product by a series of small incremental realised deformations [1]. ISF is carried out by using a rotational spherical forming tool with a rounded tip, controlled by a CNC machine-tool. Because ISF is a slow process compared to conventional forming technique such as stamping, it is an especially attractive process for small batch production. ISF allows the set-up time of element manufacturing and the cost of manufacturing to be reduced. The main advantages of single point incremental forming are that much less forming force is required compared to conventional deep drawing and that it provides the ability to shape elements on a conventional CNC milling machine [2,3].

The essence of the process is to form the element by the integration of two tool movements: a horizontal one along a closed trajectory; and an inward transition to the next horizontal forming path. In ISF processes there is local contact of the forming tool with the sheet so that the degree of sheet deformation can be controlled in those areas exposed to excessive forming limit strains. In most methods of incremental sheet forming, the rotational speed of the forming tool is in the range of 200 to 800 rpm. The linear motion of the forming tool depends on the technological characteristics of the process and the geometry of the drawpiece, and they are usually in the range of 300-2000 mm · min^{-1} [4,5]. With increased production of thin-walled structures for automobiles and aircrafts, ISF inevitably encounters challenges in processing so-called 'lightweight' materials which are hard-to-form in cold working conditions. In order to improve material formability, a series of studies have been conducted to carry out frictional stir-assisted SPIF without using heating equipment. The frictional stir-assisted ISF processes show advantages in terms of equipment cost and process flexibility [6].

The application of lightweight components is a challenge in modern transportation engineering. Mass reduction in aircraft is necessary for ecological and economic reasons, as well as to improve product properties [7]. Aerospace components are composed of lightweight materials such as titanium, magnesium, and aluminium alloys. The 2024-T3 aluminium alloy which is the test material in this paper, is typically used in the aircraft industry ow-

[1] CARPATIAN STATE SCHOOL IN KROSNO, KROSNO, POLAND
[2] RZESZOW UNIVERSITY OF TECHNOLOGY, FACULTY OF MECHANICAL ENGINEERING AND AERONAUTICS, 12 POWSTAŃCÓW WARSZAWY AV., 35-959, RZESZÓW, POLAND
[3] TECHNICAL UNIVERSITY OF KOŠICE, KOŠICE, SLOVAKIA

* Corresponding author: tomtrz@prz.edu.pl

© 2022. The Author(s). This is an open-access article distributed under the terms of the Creative Commons Attribution-NonCommercial License (CC BY-NC 4.0, https://creativecommons.org/licenses/by-nc/4.0/deed.en which permits the use, redistribution of the material in any medium or format, transforming and building upon the material, provided that the article is properly cited, the use is noncommercial, and no modifications or adaptations are made.

ing to its high formability and high fatigue resistance. The formability of annealed and pre-aged 2024 aluminium alloy sheets in the ISF process is investigated by Hussain et al. [8]. They found that the interaction of feed pitch and tool radius is very significant for formability. It was also noted that a variation in the forming speed does not affect the formability of the annealed 2024 sheet. Furthermore, an increase in forming speed decreases the formability of a pre-aged 2024 alloy sheet. Ambrogio et al. [9] studied the formability of 2024-T3 aluminium alloy sheets by supplying a continuous current in order to generate local heating. It was found that local heating of the sheet and induced strain lead to changes in the microstructure. Li et al. [10] studied the formability of 2024-T3 aluminium alloy sheets in single-point incremental forming. It was found that surface roughness can be reduced by increasing tool diameter. Wang et al. [11] studied the effects of different process parameters on the incremental forming limit of 2024 aluminium alloy sheets in different heat treatment conditions through tensile and warm incremental forming experiments. It was found that a lower pitch value, and larger feed rate can make a component with a greater forming limit. Formability of 2024-T3 aluminium alloy sheets in SPIF were also investigated by Centeno et al. [12]. They concluded that the bending effect in SPIF, controlled by the ratio of sheet thickness to tool tip radius, might not be enough to explain the enhanced formability registered in incremental forming. Bayram and Köksal [13] formed 2024-T3 sheets using the SPIF method. Among the forming process parameters, tool path, step size and lubrication parameters were changed. The tool diameter, feed rate and spindle speed parameters were kept constant. It is clear from the results that a tool path that spirals and always keeps in touch is more successful than a tool path that makes it an incremental process. Ruszkiewicz et al. [14] demonstrated how incrementally forming a stiffener of the desired geometry on the outside will manipulate the stress concentrations in the metal, and effectively reduce the amount of global springback of 2024-T3 aluminium alloy drawpieces. By stiffening the workpiece with formed stiffeners it was possible to move these stress concentrations allowing for greater control of global springback. Duflou et al. [15] investigated the influence of process parameters as well as the lubrication and geometry of the 3000 series aluminium alloy part on the forming forces. It was found that vertical step size has the least significant impact and can therefore be increased without great penalty in favour of shorter part production times. It is necessary to know the magnitude of the forming forces when trying to determine if the equipment available is capable of Forming Sheet using SPIF [16]. Mohammadi et al. [17] established general guidelines for minimising the number of test required to determine the optimum process parameters in terms of formability of an automotive aluminium alloy (AA5182-O) for laser assisted SPIF. It was found that the partial stress-relief annealing of the deformed geometry during the approach of the forming tool, is responsible for formability enhancement. Adams and Jeswiet [18] used electrically assisted SPIF to improve formability of 6061-T6 aluminium alloy sheets. Spalling and surface roughness are shown to be directly affected by current threshold density. Duflou et al. [19] and Jeswiet et al. [20] provided an overview of the body of knowledge with respect to SPIF and of corresponding conclusions on scientific progress and the outlook for further expected developments.The research presented in the literature is mainly based on the SPIF of sheets which are not covered with a soft anti-corrosion coating. The SPIF parameters should ensure the continuity of the protective layer after forming. This is especially important when forming sheets of high-strength EN AW-2024-T3 Alclad aluminium alloys commonly used in aircraft structures. The change in the thickness of the soft Alclad (technically pure aluminium) is related to the deformation of the core material and the mechanical interaction of the spherical end of the tool. Alclad 2024-T3 aluminium alloy material is difficult to form in conventional cold forming. Therefore the SPIF process of Alclad sheets is different from that commonly studied in the literature and in this paper an analysis has been carried out of the change in surface roughness during the forming of rib-stiffened panels made of aluminium alloy Alclad sheets. The article also examines the experimental verification of the possibility of using incremental sheet forming to form stiffened ribs in Alclad 2024-T3 aluminium alloy panels. Moreover, FE-based numerical computations of the SPIF process have been carried out. The numerical results have been verified based on the experimental results of the thickness distribution in the stiffened rib.

2. Experimental work

Alclad 2024-T3 precipitation-hardenable aluminium alloy sheets with a thickness of 0.4 mm were used for the fabrication of bead-stiffened panels. The nominal chemical composition of 2024 aluminium alloy is listed in TABLE 1. The values of the basic mechanical parameters (TABLE 2) were determined by tensile testing according to the ISO 6892-1:2016 standard [21]. The test specimens were cut at an angle of 0º, 45º and 90º with respect to the rolling direction of the sheet metal. The main mechanical parameters determined through tensile tests are: the yield stress $R_{p0.2}$, ultimate tensile strength R_m, elongation A_{50} and Young's modulus E. Three samples were tested for each direction, and the average values of basic mechanical parameters were determined.

TABLE 1

Nominal chemical composition (wt.%) of 2024-T3 aluminium alloy [16]

Cr	Cu	Si	Fe	Mg	Mn	Ti	Zn	Al
max. 0.1	3.8-4.9	max. 0.5	max. 0.5	1.2-1.8	0.3-0.9	max. 0.15	0.25	Rem.

TABLE 2

Mechanical properties of the 2024-T3 aluminium alloy sheets

Sample orientation	$R_{p0.2}$, MPa	R_m, MPa	A_{50}	E, GPa
0°	302.8	449.8	17.0	73.9
45°	287.6	437.9	19.8	73.2
90°	291.4	440.2	17.8	73.7

The sheets, which were tested in this study by shaping with the incremental sheet forming technology, had previously been subjected to cupping tests using the Erichsen method. The tests were performed using a dedicated Erichsen test device with a manual drive. The test parameters were in line with the guidelines set out in the standard [23]. Three repetitions were carried out. In accordance with the guidelines specified by the standard, the sheet specimen was fixed with a pressure ring, and then the punch was slowly pressed until a crack appeared in the sheet. The diameter of the spherical end of the punch was 20 mm. The value of the linear punch offset was then read, this quantity is standardised and is designated as the Erichsen cupping index (IE).

Measurement of the surface roughness parameters was carried out using a Contour GT 3D optical microscope. The main standard 3D parameters determined by this measurement (TABLE 3) are the root mean square roughness parameter *Sq*, the average roughness *Sa*, surface kurtosis *Sku*, surface skewness *Ssk*, the 10-point peak-valley surface roughness *Sz*, the highest peak of the surface *Sp*, the maximum pit depth *Sv* and the root mean square gradient *Sdq*. Fig. 1 shows the surface morphology of the original sheet and directional profiles.

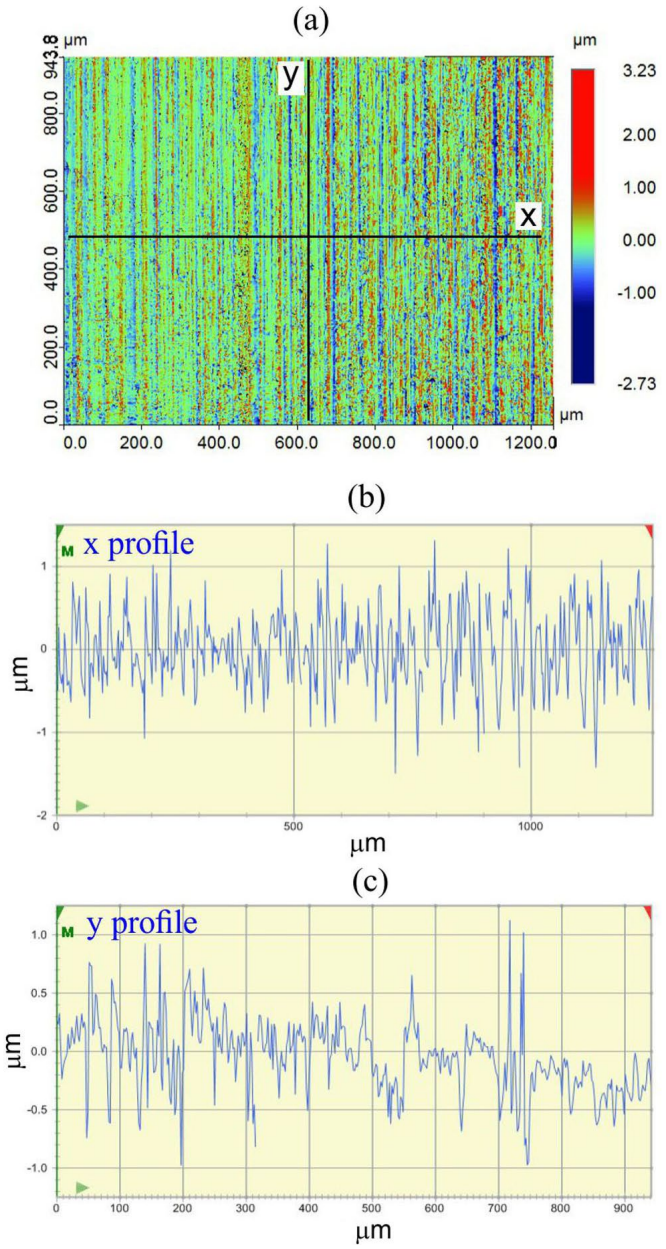

Fig. 1. Surface morphology of the specimen: (a) the original sheet, (b) and (c) are directional profiles of the surface topography

TABLE 3

Basic surface roughness parameters of 2024-T3 aluminium alloy

Sa, µm	*Sq*, µm	*Ssk*	*Sku*	*Sz*, µm	*Sp*, µm	*Sv*, µm	*Sdq*, deg
0.335	0.436	–0.017	3.794	5.961	3.231	–2.73	14.99

Trials of the forming of longitudinal U-shaped stiffening ribs (Fig. 2) by SPIF were conducted on the CNC HAAS TM1P 3-axis milling machine using a special fixture (Fig. 3) mounted on the bed of a machine tool. To reduce the contact forces on the tool tip – sheet metal interface a fully synthetic 75W85 oil (Castrol Ltd., UK) was applied. The basic properties of the oil used are: viscosity 74.0 $mm^2 \cdot s$ (at 40°C), density 874 $kg \cdot m^{-3}$ (at 15°C), freezing point –45°C. A sheet is placed in the tooling, and is clamped at the edges. Then the tool moves following the required shape in the space under CNC control, so that the part is obtained as the result of accumulated, localised, plastic deformations.

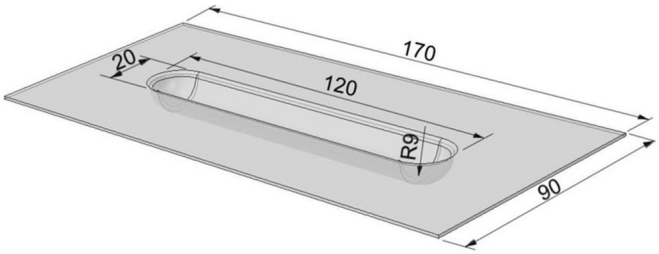

Fig. 2. Shape and dimensions of the rib-stiffened panel

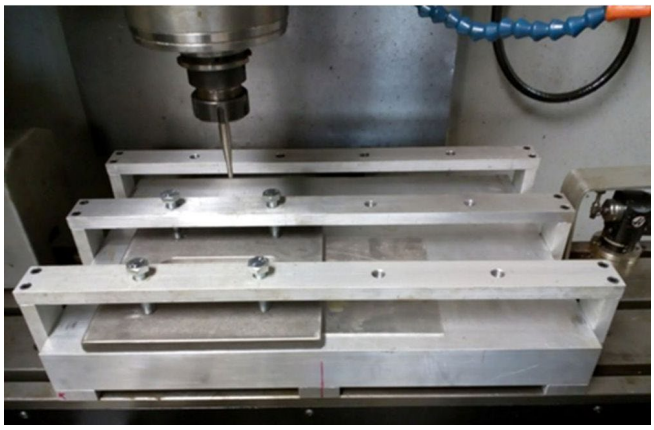

Fig. 3. Incremental sheet forming equipment

The tool with a rounded tip with a radius $R = 3.5$ mm was made of high-speed steel. The clamping of the tool in the head of the machine was achieved through the "ER" collet system, which allowed the tools to be mounted with a cylindrical shank.

The aim of the investigations was to determine the influence of the forming parameters and tool path strategy on the quality of the surface of stiffened ribs and the maximum depth of the rib prior to cracking of the sheet metal. The parameters of the SPIF process are listed in TABLE 4.

TABLE 4

Parameters of SPIF

Test no.	Feed rate, f (mm/min)	Tool rotational speed, n (rpm)	Vertical pitch a_p (mm)
T1	800	36	–0.5
T2	1500	96	–0.5
T3	800	96	–0.5
T4	1500	36	–0.5

Two tool path strategies were considered. In the first case, the tool moves downwards to the final position along a continuous path with linear vertical pitch (Fig. 4a). In the second strategy, the tool moves along multi-step paths with z-level contouring (Fig. 4b). The profile of the tool-path trajectory (Fig. 5) for the desired geometry was generated using the EdgeCAM software. After the control program was created, the forming device and the tool were mounted on the milling machine. Then the control program created in the simulation mode was validated in the test mode. Three specimens were fabricated for each set of parameters.

The surface morphology of the specimens was measured with a Talysurf CCI Lite 3D optical profiler and a Tescan model VEGA3 scanning electron microscope.

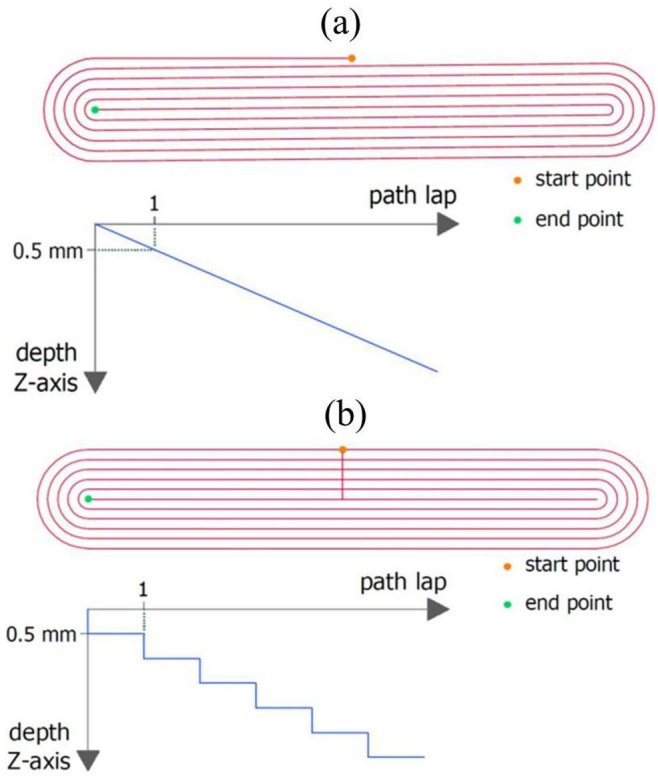

Fig. 4. Tool path strategies: (a) spiral with continuous sinking and (b) multi-step z-level contouring tool path

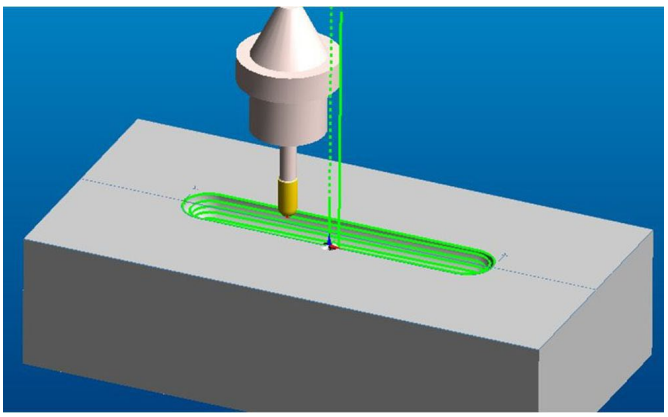

Fig. 5. Generated tool paths performed in EdgeCAM software

3. Numerical modelling

A 3D finite element (FE) model was built using the commercial FE-package ABAQUS/Standard. This section describes the FEM model in terms of geometry, mesh type, boundary conditions and material model. The results of numerical modeling of SPIF of bead-stiffened panels are presented in the next section.

The blank, die and forming tool were modelled in accordance with the experimental set-up. As the forming tool and die were considered to be rigid, no deformation was assumed in those parts during the forming process. The blankholder has not been modelled. However, the displacement of the nodes of the blank lying on the surface that is in contact with the blankholder has been fixed (Fig. 6).

An implicit time integration scheme is used to simulate the SPIF process. It is often preferred in terms of accuracy, for example, predicting the geometry achieved [24] and sheet thinning [25]. The major advantage of the implicit method is its unconditional stability. However, the major drawback of the explicit time integration algorithm is that it is conditionally stable. The size of the increment in the implicit integration scheme is only limited by the accuracy requirement and the robustness of the Newton procedure [26]. The time lapse in SPIF is of the order of minutes to hours leading to a minimum of 10^7-10^8 increments, which is a prohibitively large number [27]. For this reason, explicit simulations need more computing time than the implicit method [28].

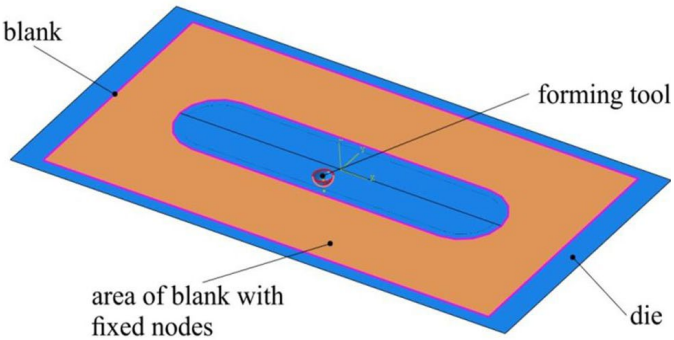

Fig. 6. Model of the tools and blank in the FE analysis

The blank was modelled with 8-node reduced integration, doubly curved shell elements called S4R in ABAQUS terminology [29]. S8R is a quadrilateral, stress/displacement shell element with reduced integration, 6 DOF per node and a large-strain formulation. Local densification of the FE mesh has been applied to the middle part of the workpiece in the area of working of the forming tool. This mesh density is chosen after testing different mesh sizes in order to achieve stability and convergence of the numerical results. The results obtained with a reference model of the layout and size of elements in the operating area of the forming tool in the range from 0.6 to 1.8 mm showed the deformation values clearly coinciding with the reduction of element size. The relative differences were less than 5% in the mesh size range of 0.5 to 0.9 mm. However, the CPU computation time in the case of element size 0.5 mm increased several times over the same range. The larger the mesh size, the smaller the time step must be to ensure adequate contact between the nodes of the workpiece and surface of the forming tool. The size value was set at 0.9 mm as a compromise between CPU time and model quality. Die and tool surfaces are modelled with 4-node bilinear discrete rigid elements R3D4. The blank model was composed of 6766 elements, while the tools consisted of 5387 elements.

The elastic behaviour in the numerical simulations is specified by the value of Young's modulus, E = 72230 MPa, and Poisson's ratio, ν = 0.33. The numerical simulations have been performed with plasticity behaviour described by the von Mises yield criterion. The isotropic hardening behaviour implemented in the FEM model uses the true stress- strain curve determined experimentally. The friction properties of the Alclad 2024-T3 aluminium alloy sheets used in the experiments have been described by penalty formulation with coefficient of friction μ = 0.15.

4. Results

This section presents the results of the experimental research on rib forming in metallic sheets made of Alclad 2024-T3 aluminium alloy using the SPIF method. Firstly, the effect of the forming parameters and tool path strategy on the possibility of forming the ribs and on the surface roughness in SPIF is presented. Secondly, the results of the formability testing are shown. And finally, the distributions of sheet thickness determined experimentally and simulated using the FE-based model are presented.

As the tool continued its movement along the tool path, a crack is not propagated to the longitudinal part of the rib (Fig. 7a). A different behaviour of the sheet was observed for the multi-step z-level contouring strategy. In this case, when the tool reached a depth of 3.53 mm (TABLE 5), a crack was formed in the corner of the rib which is the most strained region of the sheet due to the complex stress state. In contrast to the spiral strategy with continuous sinking, the crack was propagated along with the moving tool (Fig. 7b).

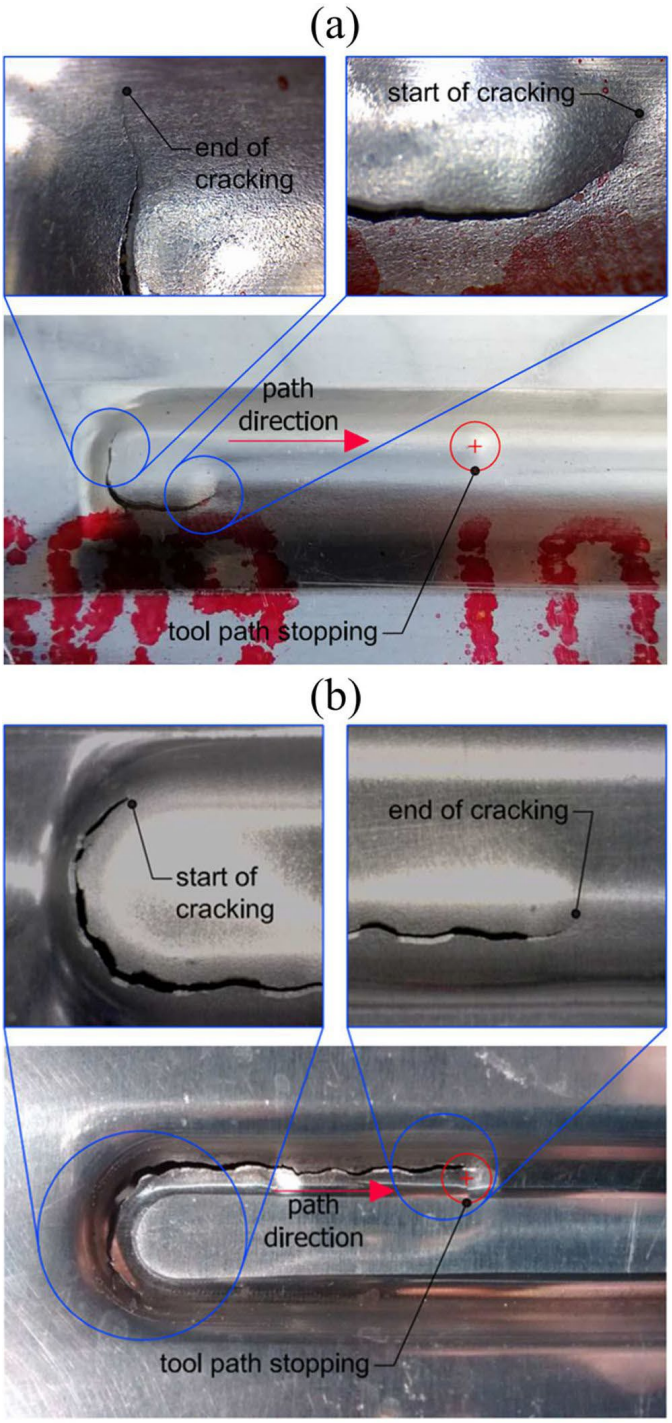

Fig. 7. Fracture at the bottom of the rib formed with (a) the spiral strategy with continuous sinking and (b) the multi-step z-level contouring strategy

TABLE 5

Effect of tool strategy on the height of rib when fracture occur

Test no.	Strategy	
	spiral with continuous sinking	multi-step z-level contouring
T1	5.53 (±0.15) mm	3.36 (±0.25) mm
T2	5.4 (±0.2) mm	3.53 (±0.15) mm
T3	5.56 (±0.11) mm	3.36 (±0.15) mm
T4	5.16 (±0.15) mm	3.4 (±0.17) mm

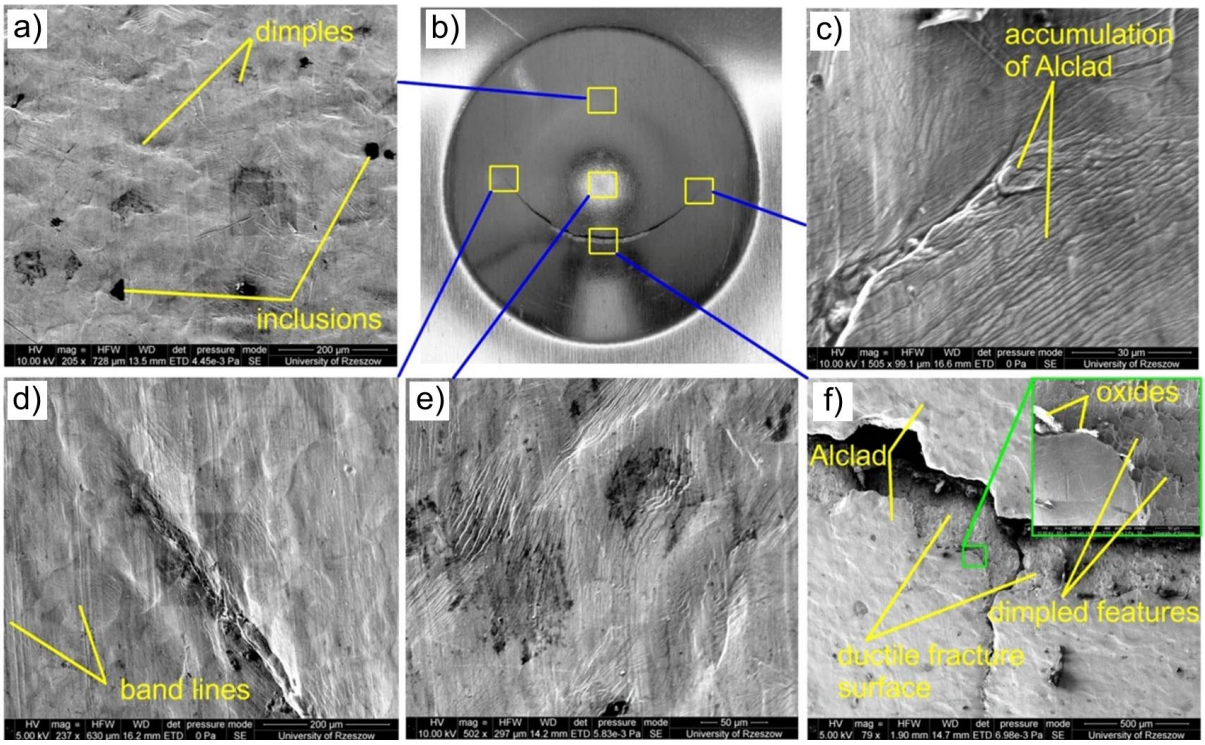

Fig. 8. Dome surface images after the appearance of a crack: a) magnification of the appearance of the lateral surface of the dome free surface; b) appearance of the dome free surface; c), d) magnification of the crack propagation region; e) magnification of the dome apex; f) magnification of the fracture region in the vicinity of the dome apex

The character of the fracture mechanism of 2024-T3 aluminium alloy sheets has been studied using the Erichsen test. The EI of the sheets tested was equal to 4.8 mm (±0.14 mm). Figure 8b shows the top view of a deformed specimen after the Erichsen test and the fracture morphologies. At a certain distance from the apex of the dome, the surface topography is characterised by distorted dimples (Fig. 8a) which increase with deformation of the sheet metal. A clear macroscopic crack is visible on the deformed specimen at a certain distance from the apex of dome where the orange peel effect (Fig. 8e) was created. The failure mechanism for Alclad material as a result of biaxial stretching becomes obvious. The Alclad layer can comprise up to 4% of the total plate thickness [30] and is assumed to carry no load, reducing the overall material specific strength by increasing the weight without contributing to the strength [31]. As stated in various studies on clad material [32], cracks are observed to be initiated at the surface of the cladding and subsequently grow to the interface (substrate/cladding). Cracks in the Alclad layer occur at various locations on the cladding surface (Fig. 8f). If the surface is riblet-structured as a result of the accumulation of Alclad (Fig. 8c), the cracks are exclusively initiated in the riblet valleys due to the notch effect (Fig. 8d) [33].

The interaction of the SPIF tool results in a poorer surface finish (Fig. 9) than in the case of the strategy with continuous sinking. The most suitable parameter with which to characterise the surface roughness in SPIF is the maximum peak to valley height (Rz) [34]. As the feed rate and tool rotational speed increased, the roughness of the surface increased and reached Rz = 11 μm (Fig. 10) to a maximum value for the combination

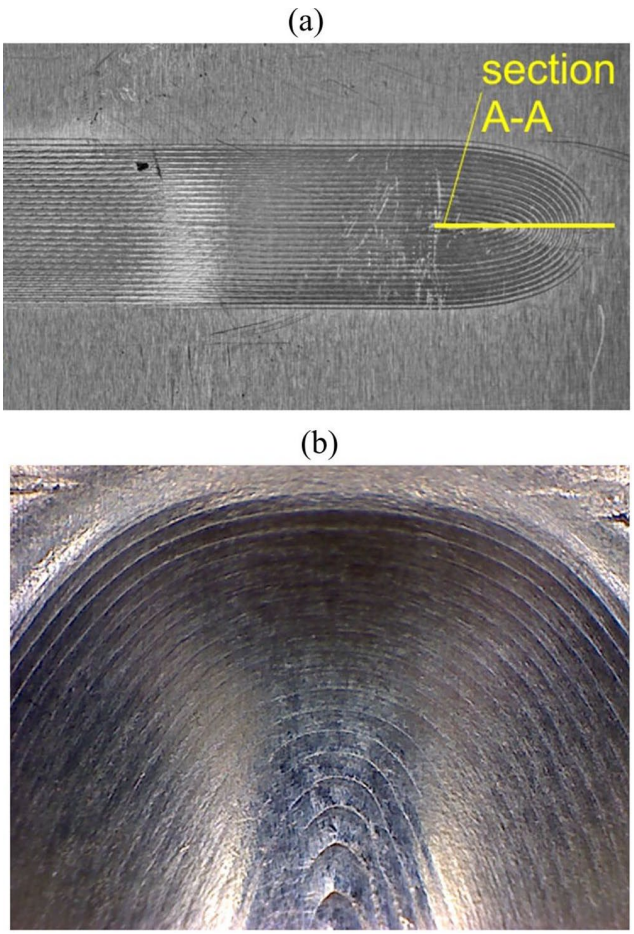

Fig. 9. View of external (a) and scratch bands (b) on the rib surface; depth of rib 5.5 mm, multi-step z-level contouring tool path

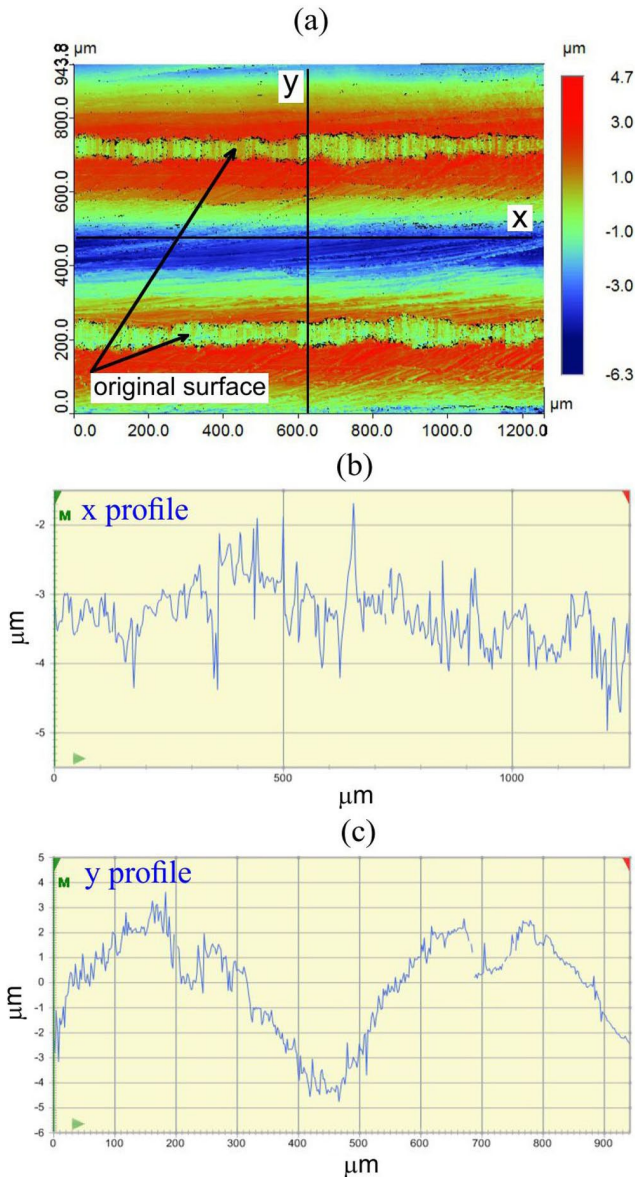

Fig. 10. Surface morphology of the specimen: (a) sheet after forming at bottom of the rib formed at parameters of T1 test with spiral strategy, (b) and (c) are directional profiles of the surface topography

of the highest value of tool rotational speed and speed rate. This is almost a two-fold increase in the maximum peak to valley height compared to the original surface. The examination of topography profiles revealed the existence of cyclic grooves separated from each other by a surface that was not in contact with the tool (Fig. 10).

The high temperature produced by the tool operation may cause severe delamination of Alclad (Fig. 11), thus causing deterioration of the clad sheet. No clear deterioration of the Alclad was observed. As also shown in Fig. 10, the final surface morphology is a combination of two effects: pile-up and sink-in. The pile-up effect causes the bulging of material around the tool tip. By contrast the sink-in effect causes the pushing of material in the direction of vertical load of the tool.

The numerical model does not take into account the criterion of crack initiation. Because the corner of the rib undergoes an excessive reduction in sheet thickness, the effectiveness of numerical simulation was validated by the results of thickness variation in the section A-A (Fig. 9a). While the tool tip moves along the desired path, there is local stress intensification. Fig. 12 shows a view of the external side of the panel thus formed. The region of local stress intensification in the workpiece material (under the tool tip) moves with the tool (Fig. 12). So, the bottom of the rib is locally deformed during tool movement.

Although, the numerical model overestimates the sheet thinning, it was observed that the sheet material is characterised by a large margin of safety in the middle part of the rib length. While the corner of the rib blank was cracked at a rib height equal to 5.5 mm, the thinning in the middle cross-section A-A (Fig. 9a) for a rib with a height of 5 mm does not exceed approximately 5.5% (Fig. 13). This gives positive premises for changing the rib profile without a reduction of panel stiffness. The mesh size value was a compromise of quality and CPU time, while assuming the deformation difference (below 6%) as an uncertainty added to the model. The deformation of the sheet in the corner of the rib may be reduced by increasing the deformation in the profile A-A. It is clear that in the case of difficult-to-deform

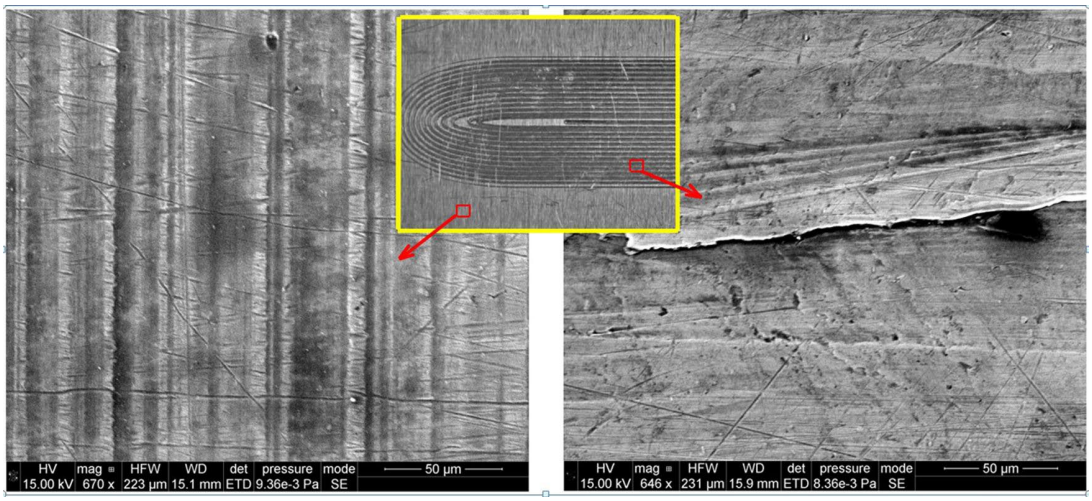

Fig. 11. SEM micrographs of the original sheet surface (left) and the sheet after forming on the lateral surface of the rib formed with the parameters of the T1 test with the spiral strategy (right)

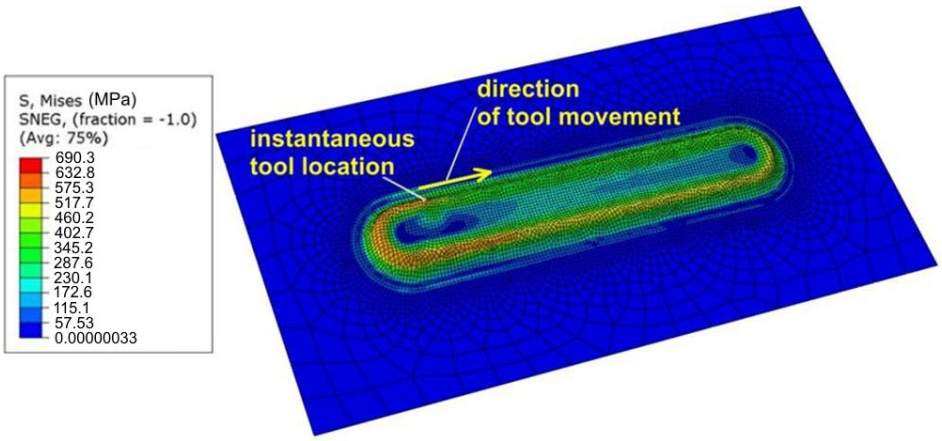

Fig. 12. Distribution of the von Mises equivalent stress in the panel formed with the parameters of the T1 model (spiral with continuous sinking)

2024-T3 aluminium alloy sheets the greatest deformation occurred in the vicinity of the contact of the tool tip with the workpiece. In the bottom of the rib the sheet deformation is smaller than in its rounded edge.

5. Discussion

Alcad is an effective way to improve the corrosion resistance of aluminium alloys. However, the forming of Alclad aluminium alloy sheets causes surface quality problems due to galling. The Alclad layer is very soft and in the case of high tool rotational speed, the tool removes a considerable amount of the workpiece resulting in poor surface quality. Experimental tests did not show discontinuities in the anticorrosive layer of the specimens despite the fact that the surface of the ribs at the point of impact of the forming tool exhibited cyclic scratch bands. In single point incremental forming processes, one of the most important features is localised deformation. The sheet is deformed locally around the contact area of the tool and sheet. As the contact area around the tool and sheet is small, high contact pressure and consequently high friction may occur [35]. This may result in poor surface finish or small linear scratch bands. Thus detailed investigation of the friction effect is necessary to improve sheet surface quality and enhance the appeal for industrial applications [36].

Tool path generation is one of the key topics in the development of ISF [37]. The results of the experimental tests allow one to conclude that the change of forming parameters within the strategy considered do not significantly affect the deformation process (TABLE 5). The use of the SPIF process with the highest feed rate would be economically justified. However, significant differences were observed between the tool paths examined. In the case of the spiral strategy with continuous sinking, the heights of the rib when fracture occurs were greater than in the case of multi-step z-level contouring. The region of crack initiation of

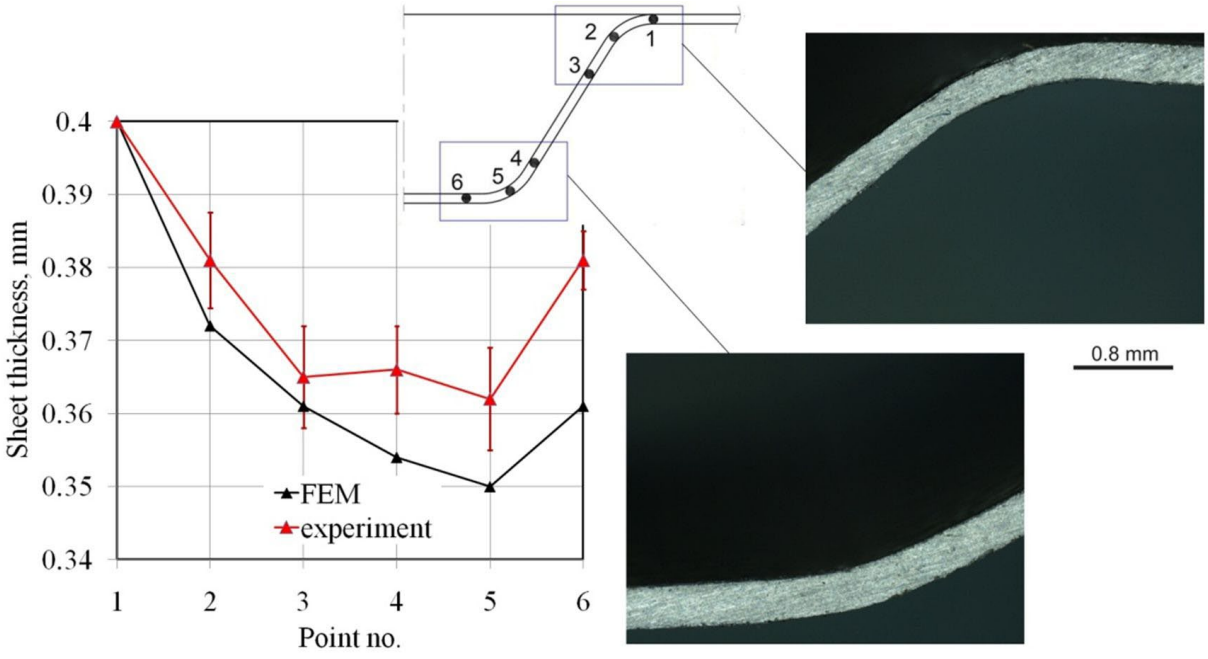

Fig. 13. Distribution of wall thickness (a) and macrograph of the cross-section of the rib (b) with height 5 mm

the sheet metal in the rib region is independent of the tool path strategy used. However, the tool path strategy influences how the crack that is initiated develop. It should be noted that the sheet metal cracking occurred in the corner of the rib, where the stress concentration occurs. A forming strategy using more material in the forming as well as the addition of a small amount of bending can greatly improve the formability [38].The fractured surface is characterised by tearing edges and deep dimples, which confirms that plastic deformation occurs during the tensile/shear test [39]. On the fracture surface a clear dimpled features are visible which confirmed a ductile fracture mode. Ductile fracture is the most common failure mode in aerospace metal alloys [40]. The ductile fracture was associated with areas of a shallow dimpled structure and cleavage of flattened grains in the proximity of oxides. The growth of micropores dominates ductile fracture which is also observed by Toda et al. [41].

6. Conclusions

The results of the numerical simulations and experimental investigations allow it to be stated that SPIF is a developmental technique for forming stiffened ribs in hard-to-form Alclad 2024-T3 aluminium alloys sheets. The following conclusions are drawn from the research:

- the main parameter which influences the formability of the sheets tested is the tool path strategy; the tool path strategy with multi-step z-level contouring allowed the formation of a rib with a depth of 3.53 mm without the risk of cracking; however the spiral strategy with continuous sinking allowed a rib with a depth of 5.56 mm to be formed,
- the change of tool rotational speed and feed rate within the strategy considered does not significantly affect the deformation process of sheet metal,
- experimental tests show that the crack initiation was observed in the vicinity of the rib corner and propagates along the bottom edge of the rib,
- the main parameter influencing the surface finish of the sheet during the SPIF process is the tool path strategy,
- localised plastic deformation in the sheet metal deforms the workpiece with higher intensity than the conventional stamping process.

Acknowledgement

The authors of this paper would like to kindly thank Dr Wojciech Bochnowski from the University of Rzeszow for the preparation of the SEM micrographs and help with surface roughness measurement.

REFERENCES

[1] Z. Liu, Int. J. Adv. Manuf. Technol. **98**, 2987-3003 (2018).
[2] Z. Chang, J. Chen, Int. J. Mach. Tool. Manuf. **146**, 103453 (2019).
[3] I. Peter, E. Fracchia, I. Canale, R. Maiorano, Procedia Manuf. **3**, 50-58 (2019).
[4] G. Fan, L. Gao, G. Hussain, Z. Wu, Int. J. Mach. Tool. Manuf. **48**, 1688-1692 (2008).
[5] M. Durante, A. Formisano, A. Langella, F.M.C. Minutolo, J. Mater. Process. Tech. **209**, 4621-4626 (2009).
[6] G. Buffa, D. Campanella, L. Fratini, Int. J. Adv. Manuf. Technol. **66**, 1343-1351 (2013).
[7] L. Zhu, N. Li, P.R.N. Childs, Propul. Power Res. **7**, 103-119 (2018).
[8] G. Hussain, L. Gao, N. Hayat, U. Dar, Int. J. Adv. Manuf. Technol. **46**, 543-549 (2010).
[9] G. Ambrogio, L. Filice, F. Gagliardi, Mater. Des. **34**, 501-508 (2012).
[10] X. Li, H. Yu, G. Guo, D. Li, AIP Conf. Proc. **1567**, 848 (2013).
[11] H. Wang, T. Wu, J. Wang, J. Li, K. Jin, Int. J. Adv. Manuf. Technol. **108**, 3507-3515 (2020).
[12] G. Centeno, A.J. Martínez-Donaire, C. Vallellano, L.H. Martínez-Palmeth, D. Morales, C. Suntaxi, F.J. García-Lomas, Procedia Eng. **63**, 650-658 (2013).
[13] H. Bayram, N.S. Köksal, Mater. Technol. **51**, 111-116 (2017).
[14] B.J. Ruszkiewicz, S.S. Dodds, Z.C. Reese, J.T. Roth, I. Ragai, Incrementally formed stiffeners effect on the reduction of springback in 2024-T3 aluminium after single point incremental forming. Proceedings of the ASME 2015 International Manufacturing Science and Engineering Conference MSEC2015, June 8-12, Charlotte (2015).
[15] J.R. Duflou, Y. Tunçkol, A. Szekeres, P.J. Vanherck, Mater. Process. Technol. **189** (1-3), 65-72 (2007).
[16] J. Jeswiet, J.R. Duflou, A. Szekeres, Adv. Mater. Res. **6-8**, 449-456 (2005).
[17] A. Mohammadi, H. Vanhove, A. van Bael, D. Weise, J.R. Duflou, Key Eng. Mater. **639**, 195-202 (2015).
[18] D. Adams, J. Jeswiet, Proc. Inst. Mech. Eng, Part B: J. Eng. Manuf. **228** (7), 757-764 (2014).
[19] J.R. Duflou, A.M. Habraken, J. Cao, R. Malhorta, M. Bambach, D. Adams, H. Vanhove, A. Mohammadi, J. Jeswiet, Int. J. Mater. Form. **11**, 743-773 (2018).
[20] J. Jeswiet, F. Micari, G. Hirt, A. Bramley, J. Duflou, J. Allwood, CIRP Annals **54** (2), 88-114 (2005).
[21] ISO 6892-1 – Metallic materials – Tensile testing – Part 1: Method of Test at Room Temperature, International Organization for Standardization, Geneva (2016).
[22] G.E. Totten, D.S. MacKenzie, Handbook of aluminum, alloy production and materials manufacturing, CRC Press, Boca Raton (2003).
[23] ISO 20482 – Metallic materials – Sheet and strip – Erichsen cupping test, International Organization for Standardization, Geneva (2013).
[24] M. Bambach, J. Ames, M. Azaouzi, L. Compagne, G. Hirt, J.L. Batoz, Initial experimental and numerical investigationsinto a class of new strategies for single point incremental sheet forming (SPIF). The 8th International ESAFORMConference on Material Forming, Cluj-Napoca, Romania, 27th-29th April 2005, pp. 671-674 (2005).
[25] G. Ambrogio, L. Filice, F. Gagliardi, F. Micari, Adv. Mater. Res. **6-8**, 479-486 (2005).

[26] T. Belytschko, W.K. Liu, B. Moran, Nonlinear Finite Elements for Continua and Structures, John Wiley and Sons Ltd., New York (2007).

[27] A. Hadoush, A.H. van den Boogaard, Int. J. Num. Meth. Eng. **90** (5), 597-612 (2012).

[28] C. Henrard, PhD Thesis, Numerical Simulation of the Single Point Incremental Forming Process, University of Liege, Liege, Belgium (2008).

[29] Abaqus – theory manual, Dassault Systèmes, Vélizy-Villacoublay (2016).

[30] LCOA Mill Products Inc., Alloy 7075 sheet and plate, 2001.

[31] E. Randell, A. Hsiano, J. Shirokoff, Adv. Mater. Sci. Eng. **2017**, 5282659 (2017).

[32] A. Merati, Int. J. Fatigue **27**, 33-44 (2005).

[33] S. Stille, Very high cycle fatigue behaviour of riblet structured high strength aluminum alloy thin sheets, Forschungszentrum Jülich GmbH, Jülich (2015).

[34] X. Li, K. Han, Z. Li, D. Li, L. Zhang, Procedia Eng. **207**, 842-847 (2017).

[35] M. Bambach, G. Hirt, S. Junk, Modelling and experimental evaluation of thincremental CNC sheet metal forming process, in: Proceedings 7th COMPLAS, Barcelona, Spain, April 7-10, 2003.

[36] B. Lu, Y. Fang, D.K. Xu, J. Chen, H. Ou, N.H. Moser, J. Cao, Int. J. Mach. Tools Manuf. **85**, 14-29 (2014).

[37] Z. Liu, Y. Li, P.A. Meehan, Int. J. Adv. Manuf. Technol. **75**, 395-409 (2014).

[38] Z.B. Liu, Y.L. Li, P.A. Meehan, Mater. Manuf. Process. **28** (5), 562-571 (2013)

[39] Y.X. Huang, B. Han, Y. Tian, H.J. Liu, S.X. Lv, J.C. Feng, J.S. Leng, Y. Li, Sci. Technol. Weld. Join. **16**, 497-501 (2011).

[40] A.P. Mouritz, Introduction to aerospace materials, Woodhead Publishing Ltd., Oxford (2012).

[41] H. Toda, H. Oogo, K. Horikawa, K. Uesugi, A. Takeuchu, Y. Suzuki, M. Nakazawa, Y. Aoki, M. Kobayashi, Metall. Mater. Trans. A **45**, 765-776 (2014).